Optik - International Journal for Light and Electron Optics 272 (2023) 170264

Contents lists available at ScienceDirect

Optik

journal homepage: www.elsevier.com/locate/ijleo

Analytical correction of pupil-offset off-axis telescopes with complex figure errors and misalignments based on nodal aberration theory

Ming Wen, Hongcai Ma *, Chengshan Han

Changchun Institute of Optics, Fine Mechanics and Physics, Chinese Academy of Sciences, Changchun 130033, China

ARTICLE INFO

Keywords:
Off-axis reflective telescope
Active optics
Correction
Nodal aberration theory

ABSTRACT

Active optical correction is necessary for space large-aperture optical telescopes, especially for systems with high performance requirements. This paper proposes an analytic correction method for pupil-offset off-axis optical telescopes with misalignments and complex figure errors on the basis of nodal aberration theory (NAT). An analytical description of the wave aberration contribution from the complex surfaces in off-axis telescopes is derived, which gives a unified description for the impacts of the complex surfaces located at the stop and away from the stop. Using the analytical description, a correction model for off-axis telescopes with figure errors and misalignments is established. The off-axis optical telescope with trefoil and astigmatic figure errors and lateral misalignments is taken as a typical example, the presented method is discussed. After the corresponding correction, the perturbed off-axis telescope is almost restored to the system nominal states, which can meet the specification requirements well. Finally, the Monte Carlo simulations are implemented to demonstrate the effectiveness of the presented approach.

1. Introduction

Reflective telescopes, compared with refractive telescopes, have the merits of no chromatic aberrations, wide spectrum, high transmission, etc. Owing to weight constraints, the mirrors and supporting structures of space-based systems will need to be lightweight. This sort of system is susceptible to some harsh environments, such as strong vibration and heat stress, which can degrade system performance. As the system aperture size increase, it is essential to equip the active optical system [1–4] to correct system perturbations (element misalignments and surface deformations). Generally speaking, the types and values of perturbations will increase with increase of the surface size, especially when there are strict constraints on weight and cost of optical systems. As the system aperture becomes larger and larger, other mirrors besides the primary mirror become larger and larger. Therefore, there may be figure errors on mirrors located away from system stop. And the influence of these figure errors on the wave aberration also needs to be considered. In the on-axis telescopes, the obscuration of the mirrors and the spider limits signal-to-noise ratio, energy concentration, etc. In order to overcome the shortcomings of on-axis telescopes, off-axis systems have been presented [5,6]. However, the system aberration properties become more complicated because the system symmetry is broken. So the correction of perturbed off-axis telescopes become very difficult. For telescope correction, the perturbed optical elements can be directly corrected. The telescopes can also be corrected at the system pupil plane or the plane conjugated to the pupil based on the principles of adaptive optics [7,8].

* Corresponding author.
E-mail address: mahc@ciomp.ac.cn (H. Ma).

https://doi.org/10.1016/j.ijleo.2022.170264
Received 5 June 2022; Received in revised form 10 October 2022; Accepted 16 November 2022
Available online 17 November 2022

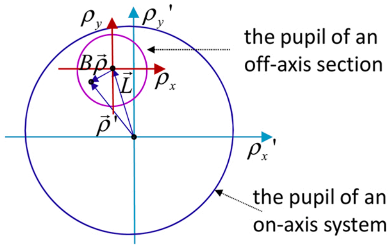

Fig. 1. Relationship between the decentered and parent pupil vector.

In order to correct disturbed telescopes, the relevant correction values need to be determined. Several methods have been reported to obtain these correction values, such as reverse optimization method (ROM), sensitivity table method (STM) and NAT-based method. The ROM [9] utilizes the function module of optimization in optical analysis software to get the correction values. It is convenient on the ground. However, the approach is difficult to carry out in space orbit. Among them methods, STM is widely applied [10]. The STM mainly uses linear-based approximation, so the corresponding accuracy is restricted by the hypothesis. If the perturbation range grows, the correction values calculated by using STM may be inexact. In addition, perturbation parameters in some systems may be strong coupling, which can bring about the corresponding singular problem in STM, and calculated correction values can also be inaccurate. Moreover, most of correction approaches are numerical. These numerical approaches are hard to provide in-depth theoretical guidance for optical correction. In practical engineering application, there are some blind problems. In order to overcome the weaknesses, The NAT-based method is presented.

Nodal aberration theory, developed by R. V. Shack and K. P. Thompson et al. [11–16], is a very effective theory for analysis and alignment of asymmetric systems. Recently, some discussions on the correction strategy for perturbed reflective telescopes based on NAT have been reported [17–24]. In reference [17], an analytical method was proposed to separate influences of misalignments from astigmatic surface figure errors. It discussed the influences of the primary mirror figure errors on the total aberration, but did not give the discussion on influences of the surface figure errors away from the system stop. In references [18,19], the influences of freeform surfaces on wave aberration of on-axis systems was discussed. The field dependence of wave aberration contribution of freeform surfaces away from the system stop was presented. In reference [20], the impact of the figure errors of the large aperture mirror on the wave aberration was discussed, which adopted the method based on scalar pupil coordinate transformation. It is difficult to be extended to the optical telescope with surface high-order figure errors. In reference [21], the influence of figure errors on the wave aberration of the on-axis telescopes was mainly discussed, and determination of trefoil and astigmatic figure errors and misalignments for on-axis telescopes was given. In references [22–24], the determination of misalignments for reflective telescopes was mainly discussed, and there are few discussions on surface figure errors. However, these references do not give the analytical description for the influences of the freeform surfaces away from the system stop in off-axis telescopes, and the corresponding correction approach of off-axis optical systems with complex figure errors and element misalignments is not given. Therefore, the paper first discusses the influences of freeform surfaces located away from system stop on wave aberration in off-axis telescopes, and then gives the correction model for off-axis systems with complex figure errors and misalignments on the basis of NAT.

The article is organized as follows. Section 2 gives a field-dependent aberration formulation of freeform surfaces for off-axis telescopes. In Section 3, the correction model of off-axis systems with complex figure errors and misalignments on the basis of NAT is developed. In Section 4, the determination and analysis of correction values of disturbed off-axis two-mirror systems are demonstrated. In Section 5, the paper is concluded.

2. Wave aberration function and field-dependent aberration formulation of freeform surfaces in perturbed off-axis telescopes

2.1. Vector aberration function in perturbed off-axis telescopes

The corresponding aberration contribution of all surfaces in optical systems should be considered. In rotationally symmetric optical systems, the vector wave aberration expression can be given by [13].

$$W = \sum_{j}\sum_{p}^{\infty}\sum_{n}^{\infty}\sum_{m}^{\infty}(W_{klm})_j\left(\vec{H}\cdot\vec{H}\right)^p(\vec{\rho}\cdot\vec{\rho})^n\left(\vec{H}\cdot\vec{\rho}\right)^m, \tag{1}$$

where $l = 2n + m$ and $k = 2p + m$, $\vec{\rho}$ designates the normalized pupil vector, $\vec{H}$ designates the normalized field vector, $(W_{klm})_j$ designates the corresponding aberration coefficient.

The pupil-offset off-axis system referred to in the paper can be seen as an off-axis part of the rotationally symmetric optical system, which is also called the off-axis system. As illustrated in Fig. 1, the vector relationship between the decentered and parent pupil vector can be given by

$$\vec{\rho}' = B\vec{\rho} + \vec{L}, \tag{2}$$

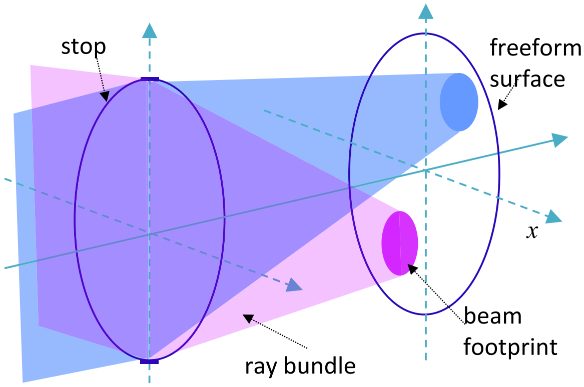

Fig. 2. Diagram of the freeform surface that is located away from system stop.

where $\overrightarrow{L}$ represents the pupil decentered vector that is normalized by the radius of the parent pupil, B designates the scaling factor, $\overrightarrow{\rho}'$ denotes the parent pupil vector, $\overrightarrow{\rho}$ designates the decentered pupil vector of the decentered system.

The aberration representation of the decentered pupil optical system without misalignment were reported in [25,26]. In the misaligned system, to obtain the expression of aberration field, the effective field vector was proposed [27], which can be expressed as

$$\overrightarrow{H}_{Aj} = \overrightarrow{H} - \overrightarrow{\sigma}_j, \tag{3}$$

where j is the surface serial number, $\overrightarrow{\sigma}_j$ designates the decenter vector of aberration field, which is connected with the corresponding parameters of the misaligned system.

In misaligned off-axis systems, the vector form of the wave aberration function is given by

$$W = \sum_j \sum_p^\infty \sum_n^\infty \sum_m^\infty (W_{klm})_j \left(\overrightarrow{H}_{Aj}\cdot\overrightarrow{H}_{Aj}\right)^p \left[\left(B\overrightarrow{\rho}+\overrightarrow{L}\right)\cdot\left(B\overrightarrow{\rho}+\overrightarrow{L}\right)\right]^n \left[\overrightarrow{H}_{Aj}\cdot\left(B\overrightarrow{\rho}+\overrightarrow{L}\right)\right]^m. \tag{4}$$

2.2. Quantitative description of field-dependent aberration contribution from freeform surfaces in perturbed off-axis telescopes

The freeform surface generally refers to rotationally nonsymmetric surface, which cannot be expressed by spherical and aspheric coefficients. There are some ways to define freeform surface at present, each of which has its own advantages. One of common definitions is that a freeform optical surface is equivalent to the sum of a conic base and a ϕ-polynomial overlay (Zernike polynomials). But here, to facilitate the discussion, the freeform surface or complex surface figure error denotes the ϕ-polynomial overlay, excluding the base conic. The advantage of Zernike polynomials is the orthogonality of surface description, and they can be easily associated with the corresponding geometrical aberrations [28]. In this case, the freeform surface may be regarded as the zero-power optical thin plate, which only affects the wave aberration characteristics, but does not affect the first-order characteristics of the system. Especially for large reflective telescopes, supposing a typically small FOV, it can be considered that the contribution of the freeform surface to system aberration is related to the location of the footprint on the surface and not dependent on the incidence angle. Since the freeform surface has no rotational symmetry, its contribution at a certain point is related to radial component and azimuthal component of the surface. On the basis of nodal aberration theory, the wave aberration contribution of freeform surface can be described by the vector method. The main purpose of this section is to give an analytical description for wave aberration contribution of freeform surface in off-axis telescopes, which can be used in engineering practice. The description with clear physical meaning is discussed here, not for pure mathematical derivation. In this paper, the surface with complex figure errors can be regarded as the freeform surface.

If the freeform surface in an off-axis telescope is located at the system stop, the corresponding beam footprint covers the whole surface, which is the same for every field point. In this case, it can be considered that the aberration contributions of the freeform surface in different field points are the same. Its contribution can be expressed as

$$W_i(\overrightarrow{\rho}) = \left(n_i' - n_i\right)\sum_j C_j\cdot Z_j(\overrightarrow{\rho}), \tag{5}$$

where $W_i(\overrightarrow{\rho})$ denotes the aberration contribution from freeform overlay, $Z_j(\overrightarrow{\rho})$ designates the Zernike polynomials, C_j denotes the corresponding Zernike coefficient, $n_i'$and n_i denotes the refraction (reflection) indices after and before the surface i.

If the freeform surface in an off-axis telescope is away from system stop, the corresponding footprint of light beam at each field point just covers a certain portion of the surface, which is shown in Fig. 2. The location of the beam footprint is related to the coordinate of the field point, so the wave aberration contribution is also related to the coordinate of the field point. The vector relationship between the beam footprint and the freeform surface away from system stop in off-axis systems is shown in Fig. 3. As a typically small

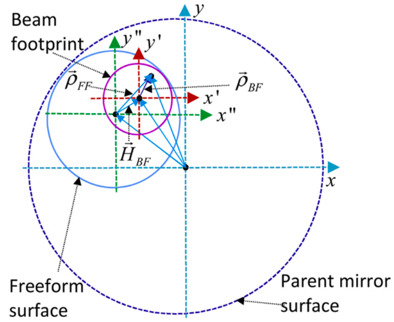

Fig. 3. Relationship between the beam footprint and the freeform surface that is located away from system stop in off-axis systems.

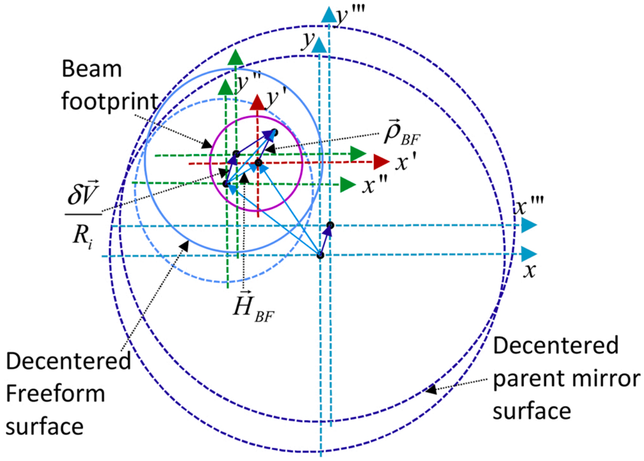

Fig. 4. Relationship between the beam footprint and freeform surface decentered from the reference axis and located away from the stop in off-axis systems.

FOV, the aberration contribution from the freeform overlay in off-axis systems can be given by

$$\begin{aligned} W_i(\vec{\rho}) &= \left(n_i' - n_i\right)\sum_j C_j \cdot Z_j\left(\vec{\rho}_{BF} + \vec{H}_{BF}\right) \\ &= \left(n_i' - n_i\right)\sum_j C_j \cdot Z_j\left(\frac{r_i}{R_i}\vec{\rho}' + \frac{\bar{y}_i}{R_i}\vec{H}\right) \end{aligned} \tag{6}$$

where $\vec{\rho}_{BF}$ denotes the scaled aperture vector that is normalized by the corresponding radius of freeform surface, $\vec{H}_{BF}$ represents the aperture decentered vector that is normalized by the surface radius, r_i is the radius of the beam footprint, R_i is the radius of freeform surface, $\bar{y}_i$ designates the height of the paraxial chief ray relative to the corresponding optical axis ray, $\vec{\rho}'$ designates the scaled aperture vector normalized by the beam footprint radius. In Eq. (6), the net contribution of wave aberration from the freeform overlay is field dependent. If the freeform surface is at the system stop, $r_i/R_i = 1, \ \bar{y}_i/R_i = 0$. Therefore, the Eq. (6) can describe the contribution of wave aberration from the freeform overlay considering all the surfaces (located at the stop and away from the stop) in off-axis telescopes.

When the surface is decentered from the corresponding mechanical reference axis, the beam footprint of a certain field relative to the mechanical reference axis remains unchanged. However, the beam footprint will change relative to the decentered surface. The corresponding relationship between the beam footprint and the surface decentered from the mechanical reference axis and located away from the stop in off-axis systems is illustrated in Fig. 4. In off-axis systems, the wave aberration contribution from the decentered freeform surface is expressed as

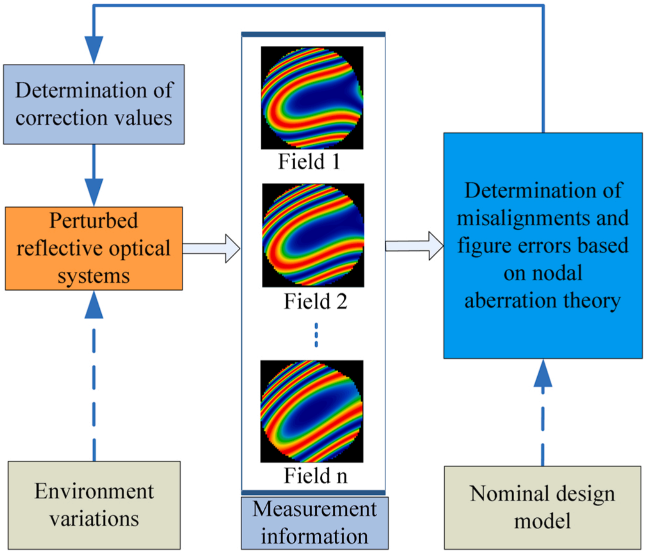

Fig. 5. Schematic diagram of correction process for perturbed reflective telescopes.

$$\begin{aligned} W_i\left(\vec{\rho}', \vec{H}\right) &= \left(n_i' - n_i\right)\sum_j C_j \cdot Z_j\left(\vec{\rho}_{BF} + \vec{H}_{BF} - \frac{\delta\vec{V}}{R_i}\right) \\ &= \left(n_i' - n_i\right)\sum_j C_j \cdot Z_j\left(\frac{r_i}{R_i}\vec{\rho}' + \frac{\bar{y}_i}{R_i}\vec{H} - \frac{\delta\vec{V}}{R_i}\right) \\ &= \left(n_i' - n_i\right)\sum_j C_j \cdot Z_j\left[\frac{r_i}{R_i}\vec{\rho}' + \frac{\bar{y}_i}{R_i}\left(\vec{H} - \frac{\delta\vec{V}}{\bar{y}_i}\right)\right] \end{aligned} \tag{7}$$

where $\delta\vec{V}/R_i$ denotes the surface displacement vector relative to the reference axis normalized by the radius of the freeform surface. In this section, we can also discuss the off-axis systems with the freeform surface in the framework of the parent system, and the results are consistent with the above results.

3. Correction model for off-axis telescopes with figure errors and misalignments on the basis of NAT

The surface shape and position of optical elements can be adjusted by using the corresponding mechanisms in active optical systems. In the adjustment process, the correction values of optical components need to be determined accurately. Schematic diagram of correction process for perturbed reflective telescopes is shown in Fig. 5. The key of the correction process is to obtain the correction values.

The previous section gives the quantitative description of wave aberration contribution from the complex surfaces in off-axis systems. In this section, the correction method of off-axis telescopes with complex figure errors and misalignments will be discussed. The following discussion is divided into two different cases. One is the case of the misaligned surface without figure errors, and the other is the case of the misaligned surface with figure errors.

Here, the case of the misaligned surface without figure errors in off-axis systems is firstly considered. According to the relevant rules of vector multiplication, some fifth-order aberration expressions in misaligned off-axis telescopes in vector form can be obtained [29,30]. Based on the relationships between the fifth order expansion and Zernike polynomials, the optical correction model of misaligned off-axis telescopes without surface figure errors based on NAT is given by

$$\begin{cases} B^2\left(\vec{\Psi}^2_{222} + \vec{\Psi}^2_{422}\right) = 2\vec{C}_{W22} \\ B^3\left(\vec{\Psi}_{131} + \vec{\Psi}_{331M}\right) = 3\vec{C}_{W31} \\ B^3\vec{\Psi}^3_{333} = 4\vec{C}_{W33} \\ B^4\vec{\Psi}^2_{242} = 8\vec{C}_{W42} \\ B^5\vec{\Psi}_{151} = 10\vec{C}_{W51} \end{cases} \tag{8}$$

where the definitions of the notations ($\vec{\Psi}^2_{222}, \vec{\Psi}_{131}$, etc.) is just like that in ref. [29,30], the definitions of the notations ($\vec{C}_{W22}, \vec{C}_{W31}$, etc.) is expressed as

$$\begin{cases} \vec{C}_{W22} = \begin{bmatrix} \left(\vec{C}_{5,6} - 3\vec{C}_{12,13}\right) + 12\vec{E}^2\left(C_9 - 5C_{16}\right) + 120\vec{E}^3\vec{E}^* C_{16} \\ -3\vec{E}\left(\vec{C}_{7,8} - 4\vec{C}_{14,15}\right) + 12\vec{E}\vec{E}^*\vec{C}_{12,13} - 80\vec{E}^2\left(\vec{E}\cdot\vec{C}_{14,15}\right) \\ +10\left(\vec{E}\cdot\vec{E}\right)\vec{E}\vec{C}_{14,15} + 30\vec{E}^3\left(\vec{C}_{14,15}\right)^* - 3\vec{E}^*\vec{C}_{10,11} \end{bmatrix} \\ \vec{C}_{W31} = \begin{bmatrix} \left(\vec{C}_{7,8} - 4\vec{C}_{14,15}\right) - 8\vec{E}\left(C_9 - 5C_{16}\right) - 120\left(\vec{E}\cdot\vec{E}\right)\vec{E}C_{16} \\ +40\vec{E}\left(\vec{E}\cdot\vec{C}_{14,15}\right) - 10\vec{E}^2\left(\vec{C}_{14,15}\right)^* - 4\vec{E}^*\vec{C}_{12,13} \end{bmatrix} \\ \vec{C}_{W33} = \vec{C}_{10,11} - 40\vec{E}^3 C_{16} + 10\vec{E}^2\vec{C}_{14,15} - 4\vec{E}\vec{C}_{12,13} \\ \vec{C}_{W42} = \vec{C}_{12,13} + 30\vec{E}^2 C_{16} - 5\vec{E}\vec{C}_{14,15} \\ \vec{C}_{W51} = \vec{C}_{14,15} - 12\vec{E}C_{16} \end{cases} \tag{9}$$

where $\vec{E} = \vec{L}/B$, B designates the ratio between the radius of the decentered and parent pupil, and where $\vec{C}_{5,6} = [C_5 \quad C_6]^T, \vec{C}_{7,8} = [C_7 \quad C_8]^T, \vec{C}_{10,11} = [C_{10} \quad C_{11}]^T, \vec{C}_{12,13} = [C_{12} \quad C_{13}]^T$ and $\vec{C}_{14,15} = [C_{14} \quad C_{15}]^T$ are the Fringe Zernike coefficient vectors, C_9 and C_{16} are the corresponding Fringe Zernike coefficients, the asterisk superscript designates the corresponding vector conjugate. As can be seen, the corresponding aberration relationship expressions of off-axis telescopes are more complex than that of on-axis telescopes. Owing to the effect of pupil transformation, the contribution of a certain kind of aberration of off-axis telescopes can be represented as the corresponding function of several Zernike coefficients. In Eq. (8), the left side can be viewed as the function of corresponding decenter vectors of aberration field, it is a direct correlation with misalignments of optical components. Therefore, the optical correction model of misaligned off-axis telescopes without surface figure errors based on NAT is obtained.

The case of the misaligned surface with figure errors in off-axis systems is discussed below. The correction model of misaligned off-axis telescopes with figure errors can be described on the basis of Eq. (8). In this case, the Zernike coefficient vectors on right side of Eq. (9) should be expressed as

$$\vec{C}_{i,i+1} = {}_N\vec{C}_{i,i+1} + {}_F\vec{C}_{i,i+1}, \tag{10}$$

where $\vec{C}_{i,i+1}$ denotes the vector of the corresponding Zernike coefficients in misaligned off-axis telescopes with figure errors, ${}_N\vec{C}_{i,i}+1$ represents the vector of the Zernike coefficients in misaligned off-axis telescopes without surface figure errors, ${}_F\vec{C}_{i,i}+1$ represents the vector of the Zernike coefficients contributed from the corresponding figure errors, which can be expressed as

$${}_F\vec{C}_{i,i+1} = {}_F\vec{C}^{PM}_{i,i+1} + {}_F\vec{C}^{SM}_{i,i+1} + \ldots, \tag{11}$$

where ${}_F\vec{C}_{i,i}+1^{PM}$ denotes the contribution of the Zernike coefficient vector from the primary mirror figure errors, ${}_F\vec{C}_{i,i}+1^{SM}$ represents the contribution of the Zernike coefficient vector from the secondary mirror figure errors. The figure errors of other surfaces (if any) also need to be considered.

Similarly, the left side of Eq. (8) should also be corrected to add the aberration contribution of the corresponding surface figure errors. The optical correction model of misaligned off-axis telescopes with surface figure errors based on NAT can be expressed as

$$\begin{cases} B^2\left(\vec{\Psi}^2_{222} + \vec{\Psi}^2_{422}\right) + 2\Delta\vec{C}_{W22} = 2\vec{C}_{W22} \\ B^3\left(\vec{\Psi}_{131} + \vec{\Psi}_{331M}\right) + 3\Delta\vec{C}_{W31} = 3\vec{C}_{W31} \\ B^3\vec{\Psi}^3_{333} + 4\Delta\vec{C}_{W33} = 4\vec{C}_{W33} \\ B^4\vec{\Psi}^2_{242} + 8\Delta\vec{C}_{W42} = 8\vec{C}_{W42} \\ B^5\vec{\Psi}_{151} + 10\Delta\vec{C}_{W51} = 10\vec{C}_{W51} \end{cases} \tag{12}$$

where the notations ($\vec{C}_{W22}, \vec{C}_{W31}$, etc.) denote the corresponding functions of the Zernike coefficient vectors in misaligned off-axis telescopes with figure errors, which are shown in Eq. (9). And where the notations ($\Delta\vec{C}_{W22}, \Delta\vec{C}_{W31}$, etc.) denote the corresponding contributions from the surface figure errors, their expressions are also consistent with Eq. (9).

So far, the correction model of off-axis telescopes with complex figure errors and misalignments has been established. It is significant for operation of active optical off-axis telescopes. To further explain the above model, in the next section, the correction of perturbed off-axis two-mirror systems will be discussed.

4. Correction of perturbed off-axis two-mirror telescopes by using NAT

4.1. Determination of correction values for perturbed off-axis two-mirror telescopes

The correction model for perturbed telescopes was developed in the previous section. In the section, the off-axis two-mirror telescope with surface figure errors and misalignments will be discussed. Other types of off-axis telescopes with figure errors and misalignments can also be corrected by similar methods.

Specifically, this subsection discusses the correction model for off-axis two-mirror telescope with trefoil and astigmatic surface figure errors of the system primary mirror and trefoil figure errors of the system secondary mirror and rigid misalignments of secondary mirror. The misalignments and element figure errors can induce the same type of aberrations. There are some complex coupling effects between them. Therefore, the correction model of perturbed off-axis systems will be complex.

4.1.1. Discussions on some vector relationships

The stop is located on primary mirror (PM) in most of large aperture telescopes. So, the stop of the system to be discussed is also located on PM, and the coordinate reference is also chosen on PM. Since there is no misalignment of PM, the decenter vectors of aberration field for PM are expressed as

$$\vec{\sigma}^{sph}_{PM} = 0, \quad \vec{\sigma}^{asph}_{PM} = 0, \tag{13}$$

where $\vec{\sigma}^{sph}_{PM}$ and $\vec{\sigma}^{asph}_{PM}$ represent the decenter vectors of aberration field for PM, the superscript *asph* and *sph* represent contributions of the aspheric departure and spherical base, respectively. Based on NAT, the decenter vectors of aberration field for secondary mirror (SM) are connected with the misalignments of SM, which are expressed as

$$\vec{\sigma}^{sph}_{SM} = \frac{1}{(1 + c_{SM} d_1)\bar{u}_{PM}} \begin{bmatrix} BDE_{SM} - c_{SM} XDE_{SM} \\ -ADE_{SM} - c_{SM} YDE_{SM} \end{bmatrix}, \tag{14}$$

$$\vec{\sigma}^{asph}_{SM} = \frac{1}{d_1 \bar{u}_{PM}} \begin{bmatrix} -XDE_{SM} \\ -YDE_{SM} \end{bmatrix}, \tag{15}$$

where $\vec{\sigma}^{sph}_{SM}$ and $\vec{\sigma}^{asph}_{SM}$ represent the decenter vectors of aberration field for SM, XDE_{SM}, YDE_{SM}, ADE_{SM} and BDE_{SM} designate the corresponding misalignments of SM, $\bar{u}_{PM}$ denotes the angle of chief ray incidence, d_1 denotes the element spacing between the SM and PM, c_{SM} is surface curvature of SM. In this section, x-axis is defined as the corresponding reference axis in accord with optical testing tradition [31].

As astigmatic figure errors exist on SM, the aberration fields contributed from the astigmatic figure errors in off-axis telescopes can be represented as

$$\begin{aligned} W_F &= N_{SM} \times {}_{F,SM}\vec{C}_{5,6} \cdot \left(B_{SM}\vec{\rho} + L_{SM}\vec{H}_F\right)^2 \\ &= N_{SM} \times \left[(B_{SM})^2 {}_{F,SM}\vec{C}_{5,6} \cdot \vec{\rho}^{\,2} + 2B_{SM}L_{SM}\vec{H}_F^{\,*}\,{}_{F,SM}\vec{C}_{5,6} \cdot \vec{\rho} + (L_{SM})^2 {}_{F,SM}\vec{C}_{5,6} \cdot \left(\vec{H}_F\right)^2 \right], \end{aligned} \tag{16}$$

where ${}_{F,SM}\vec{C}_{5,6}$ denotes the astigmatic figure errors on SM, $N_{SM} = n'_{SM} - n_{SM}$, n'_{SM} and n_{SM} are the indices of reflection after and before the SM, $B_{SM} = r_{SM,\mathrm{ft}}/R_{SM}$, $L_{SM} = \bar{y}_{SM}/R_{SM}$, $r_{SM,\mathrm{ft}}$ is the radius of the beam footprint on SM, R_{SM} is the radius of SM, $\bar{y}_{SM}$ denotes the height of paraxial chief ray on SM relative to optical axis ray, $\vec{H}_F = \vec{H} - \delta\vec{V}_{SM}/\bar{y}_{SM}$ represents the effective field vector corresponding to SM, $\delta\vec{V}_{SM}$ denotes the decenter of SM relative to the reference axis.

As trefoil figure errors exist on SM, the aberration fields contributed from the trefoil figure errors in off-axis telescopes can be represented as

$$\begin{aligned} W_F &= N_{SM} \times {}_{F,SM}\vec{C}_{10,11} \cdot \left(B_{SM}\vec{\rho} + L_{SM}\vec{H}_F\right)^3 \\ &= N_{SM} \times \left[(B_{SM})^3 {}_{F,SM}\vec{C}_{10,11} \cdot \vec{\rho}^{\,3} + 3(B_{SM})^2 L_{SM}\vec{H}_F^{\,*}\,{}_{F,SM}\vec{C}_{10,11} \cdot \vec{\rho}^{\,2} + 3B_{SM}(L_{SM})^2 \left(\vec{H}_F^{\,2}\right)^* {}_{F,SM}\vec{C}_{10,11} \cdot \vec{\rho} + (L_{SM})^3 {}_{F,SM}\vec{C}_{10,11} \cdot \left(\vec{H}_F\right)^3 \right], \end{aligned} \tag{17}$$

where ${}_{F,SM}\vec{C}_{10,11}$ denotes the trefoil figure errors on SM. It can be seen that, the derived contributions comprise the aberrations of the lower and same order aperture terms.

As the off-axis telescopes with trefoil and astigmatic surface figure errors on PM and trefoil surface figure errors on SM in off-axis telescopes are considered, the astigmatic and trefoil contributions from these figure errors can be expressed as

$$
\begin{aligned}
{}_{TF}\vec{C}_{5,6} &= {}_{TF}\vec{C}_{5,6}^{PM} + {}_{TF}\vec{C}_{5,6}^{SM} \\
&= N_{PM} \times {}_{F,PM}\vec{C}_{5,6} + N_{SM} \times 3(B_{SM})^2 L_{SM} \vec{H}^{*}{}_{F,SM}\vec{C}_{10,11},
\end{aligned} \tag{18}
$$

$$
\begin{aligned}
{}_{TF}\vec{C}_{10,11} &= {}_{TF}\vec{C}_{10,11}^{PM} + {}_{TF}\vec{C}_{10,11}^{SM} \\
&= N_{PM} \times {}_{F,PM}\vec{C}_{10,11} + N_{SM} \times (B_{SM})^3 {}_{F,SM}\vec{C}_{10,11},
\end{aligned} \tag{19}
$$

where ${}_{TF}\vec{C}_{5,6}$ and ${}_{TF}\vec{C}_{10,11}$ are the total astigmatic and trefoil contributions from these figure errors, ${}_{TF}\vec{C}_{5,6}^{PM}$ and ${}_{TF}\vec{C}_{10,11}^{PM}$ are the astigmatic and trefoil contributions from the figure errors on the PM, ${}_{TF}\vec{C}_{5,6}^{SM}$ and ${}_{TF}\vec{C}_{10,11}^{SM}$ are the astigmatic and trefoil contributions from the figure errors on the SM, $N_{PM} = n'_{PM} - n_{PM}$, n'_{PM} and n_{PM} are the indices of reflection after and before the PM.

4.1.2. Determination of element misalignments

In the presence of element misalignments, the boresight error (also called pointing error) will appear. It can be combined with other equations to determine the misalignment parameters. There exists the certain relationship between the boresight error and the aberration field decenter vector related to the spherical base, which can be given by

$$
\vec{H}_P = -2d_2k\left[\bar{u}_{PM}\left(1 + d_1c_{SM}\right)\right]\vec{\sigma}_{SM}^{sph}, \tag{20}
$$

where $\vec{H}_P$ denotes the boresight error vector, k denotes the corresponding calculation factor, d_2 is the mirror spacing between the SM and the focal plane.

As the trefoil and astigmatic surface figure errors on PM and trefoil surface figure errors on SM and rigid misalignments of SM are considered, the expression of coma aberration field can be given by

$$
B^3\left(\vec{\Psi}_{131} + \vec{\Psi}_{331M}\right) = 3\vec{C}_{W31}, \tag{21}
$$

where $B = r_{PM}/R_{PM}$, r_{PM} is the radius of the system stop of the off-axis telescope, $R_{PM}$is the radius the aperture stop of the on-axis parent telescope. After some simplification, the following matrix expression can be obtained

$$
\begin{bmatrix}
-1 & 0 \\
0 & -1 \\
H_x & H_y \\
H_x^3 + H_xH_y^2 & H_x^2H_y + H_y^3 \\
-3H_x^2 - H_y^2 & -2H_xH_y \\
-2H_xH_y & -H_x^2 - 3H_y^2
\end{bmatrix}^T
\begin{bmatrix}
A_{131,x} \\ A_{131,y} \\ W_{131} \\ W_{331M} \\ A_{331M,x} \\ A_{331M,y}
\end{bmatrix}
= \frac{3}{B^3}\vec{C}_{W31}, \tag{22}
$$

where $\vec{C}_{W31}$ is the notation shown in Eq. (9), the definition of other notations is consistent with that in ref. [14]. In Eq. (22), to solve two unknown variables, $A_{131,x}$ and $A_{131,y}$, the wavefront measurements of three points are adequate. Supposing that the wavefront measurements of exceeding three field points can be obtained, these unknown variables can be solved by using the least-square principle. And then, by combining Eq. (20), the decenter vectors of aberration field, $\vec{\sigma}_{SM}^{sph}$ and $\vec{\sigma}_{SM}^{asph}$, can be obtained. On the basis of Eq. (14) and Eq. (15), the misalignments of SM can be determined.

4.1.3. Determination of surface figure errors

As the off-axis telescopes with trefoil and astigmatic surface figure errors on PM and trefoil figure errors on SM and misalignments of SM are considered, on the basis of Eq. (12) and Eq. (18), after some simplification, the expression of the astigmatic aberration field can be represented as

$$
\frac{1}{2}B^2W_{222}\vec{H}^2 - B^2\vec{A}_{222}\vec{H} + \frac{1}{2}\vec{B}_{222}^2 + 3N_{SM}(B_{SM})^2L_{SM}\vec{H}^{*}{}_{F,SM}\vec{C}_{10,11} = \vec{C}_{W22}, \tag{23}
$$

where

$$
\begin{aligned}
\vec{A}_{222} &= W_{222,SM}^{sph}\vec{\sigma}_{SM}^{sph} + W_{222,SM}^{asph}\vec{\sigma}_{SM}^{asph}, \\
\vec{B}_{222}^2 &= B^2{}_M\vec{B}_{222}^2 + \begin{bmatrix} 2N_{PM} \times {}_{F,PM}\vec{C}_{5,6} - 6N_{SM}(B_{SM})^2L_{SM}\vec{\sigma}^{*}_{F,SM}{}_{F,SM}\vec{C}_{10,11} \\ -6N_{PM}\vec{E}^{*}{}_{F,PM}\vec{C}_{10,11} - 6N_{SM}\vec{E}^{*}(B_{SM})^3{}_{F,SM}\vec{C}_{10,11} \end{bmatrix}, \\
{}_M\vec{B}_{222}^2 &= W_{222,SM}^{sph}\vec{\sigma}_{SM}^{2(sph)} + W_{222,SM}^{asph}\vec{\sigma}_{SM}^{2(asph)},
\end{aligned} \tag{24}
$$

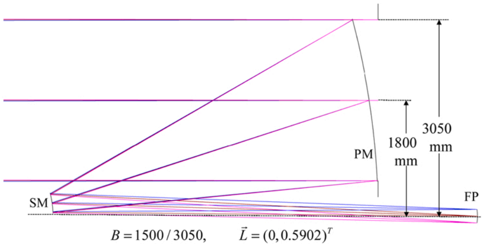

Fig. 6. Layout of the off-axis two-mirror telescope.

where $W_{222,SM}^{asph}$ and $W_{222,SM}^{sph}$ denote the astigmatic coefficients for the aspheric departure and the base spherical of SM, respectively, $\vec{\sigma}_{F,SM}$ denotes the decenter vector of aberration field for the figure errors on SM, which is given by

$$\vec{\sigma}_{F,SM} = \frac{\delta\vec{V}_{SM}}{\bar{y}_{SM}}. \tag{25}$$

According to Eq. (23), the following matrix expression can be obtained

$$\begin{bmatrix} PH_x & PH_y & \frac{1}{2} & 0 \\ -PH_y & PH_x & 0 & \frac{1}{2} \end{bmatrix} \begin{bmatrix} {}_{F,SM}C_{10} \\ {}_{F,SM}C_{11} \\ \vec{B}^2_{222,x} \\ \vec{B}^2_{222,y} \end{bmatrix} = \vec{C}_{W22} - \frac{1}{2}B^2 W_{222}\vec{H}^2 + B^2\vec{A}_{222}\vec{H}, \tag{26}$$

where $P = 3N_{SM}(B_{SM})^2 L_{SM}$, $\vec{C}_{W22}$ is the notation shown in Eq. (9). In Eq. (26), to solve two unknown vectors, $\vec{B}^2_{222}$ and ${}_{F,SM}\vec{C}_{10,11}$, the field measurements at two points are enough. Supposing that the wavefront measurements of exceeding two field points are obtained, these two unknown vectors can be solved by using the traditional least-square principle. So far, the trefoil figure errors on the SM are determined.

As the off-axis telescopes with the figure errors and misalignments mentioned above are considered, according to Eq. (12) and Eq. (19), the expression of the trefoil aberration field can be expressed as

$$\frac{1}{4}B^3 W_{333}\vec{H}^3 - \frac{3}{4}B^3\vec{H}^2\vec{A}_{333} + \frac{3}{4}B^3\vec{H}\vec{B}^2_{333} - \frac{1}{4}\vec{C}^3_{333} = \vec{C}_{W33}, \tag{27}$$

where

$$\begin{aligned} \vec{A}_{333} &= W_{333,SM}^{sph}\vec{\sigma}_{SM}^{sph} + W_{333,SM}^{asph}\vec{\sigma}_{SM}^{asph}, \\ \vec{B}^2_{333} &= W_{333,SM}^{sph}\left(\vec{\sigma}_{SM}^{sph}\right)^2 + W_{333,SM}^{asph}\left(\vec{\sigma}_{SM}^{asph}\right)^2, \\ \vec{C}^3_{333} &= {}_M\vec{C}^3_{333}B^3 - 4N_{PM}\times{}_{F,PM}\vec{C}_{10,11} - 4N_{SM}(B_{SM})^3{}_{F,SM}\vec{C}_{10,11}, \\ {}_M\vec{C}^3_{333} &= W_{333,SM}^{sph}\left(\vec{\sigma}_{SM}^{sph}\right)^3 + W_{333,SM}^{asph}\left(\vec{\sigma}_{SM}^{asph}\right)^3. \end{aligned} \tag{28}$$

where $W_{333,SM}^{asph}$ and $W_{333,SM}^{sph}$ denote the trefoil aberration coefficients for the aspheric departure and the spherical base of SM, respectively.

According to Eq. (27), after some simplification, the following matrix expression can be obtained

$$\begin{bmatrix} -3H_x^2 + 3H_y^2 & -6H_xH_y \\ 6H_xH_y & -3H_x^2 + 3H_y^2 \\ H_x^3 - 3H_xH_y^2 & 3H_x^2H_y - H_y^3 \\ -1 & 0 \\ 0 & -1 \end{bmatrix}^T \begin{bmatrix} B^3A_{333,x} \\ B^3A_{333,y} \\ B^3W_{333} \\ C^3_{333,x} \\ C^3_{333,y} \end{bmatrix} = 4\vec{C}_{W33}, \tag{29}$$

Table 1
Calculated Misalignments (Ca-M) and Introduced Misalignments (In-M) for SM.

	XDE_{SM}	YDE_{SM}	ADE_{SM}	BDE_{SM}
In-M	0.1500	-0.1500	-0.0100	0.0150
Ca-M	0.1506	-0.1512	-0.0101	0.0150

Table 2
Calculated Figure Errors (Ca-V) and Introduced Figure Errors (In-V) for PM.

	${}_F C_5^{PM}$	${}_F C_6^{PM}$	${}_F C_{10}^{PM}$	${}_F C_{11}^{PM}$
In-V	0.0600	-0.0500	0.0500	-0.0500
Ca-V	0.0602	-0.0504	0.0503	-0.0499

Table 3
Calculated Figure Errors (Ca-V) and Introduced Figure Errors (In-V) for SM.

	${}_F C_{10}^{SM}$	${}_F C_{11}^{SM}$
In-V	-0.0500	0.0500
Ca-V	-0.0502	0.0497

where $\overrightarrow{C}_{W33}$ is the notation shown in Eq. (9). To solve two unknown variables, $C_{333,x}^{3}$ and $C_{333,y}^{3}$, the wavefront measurements of three points are adequate. Supposing that the wavefront measurements of exceeding three field points can be obtained, these unknown variables can be solved by using the least-square principle. According to Eq. (28), the trefoil figure errors on PM are obtained. And then, according to Eq. (24), the astigmatic figure errors on PM are determined.

So far, the misalignments and the figure errors in off-axis telescopes have been determined, and the corresponding correction value can be obtained by taking the opposite number. Other complex surface errors in off-axis telescopes can also be determined by the similar method. It should be noted that the description accuracy of the model can be improved by optimizing the parameters used.

4.2. Verification and analysis

To verify the accuracy and effectiveness of the presented method, in this subsection, the system correction of an off-axis two-mirror telescope is demonstrated. The layout of the off-axis two-mirror telescope is illustrated in Fig. 6. The system stop is located at the PM, its exact diameter is 2500 mm. The system has a $\pm 0.1^{\circ}$ field of view. The offset of system stop is 1800 mm. The element radii of the PM and SM are $-$ 11,500.00 mm and $-$ 1414.58 mm. The conic values of the PM and SM are $-$ 1.002 and $-$ 1.498. The thickness value between PM and SM is - 5110.49 mm. To demonstrate the example, four FOVs are used, which are (0.07°, 0.07°), (-0.07°, 0.07°), (0.07°, -0.07°) and (-0.07°, -0.07°), respectively.

According to the corresponding Zernike coefficients at different field points and the boresight error of the perturbed system, the correction values of the perturbed off-axis system can be determined based on the proposed approach. The calculated and introduced misalignment values for SM are shown in Table 1. The calculated and introduced figure errors for PM are shown in Table 2. The calculated and introduced figure errors for SM are illustrated in Table 3. In practical application, the introduced figure errors (In-V) are obtained by wavefront measuring devices. The calculated figure errors (Ca-V) are the output of the correction model.

In Tables 1–3, it can be seen that the calculated and introduced values are almost identical, which show the proposed approach is effective. In order to correct the system, the opposite numbers of the calculated surface figure errors and misalignments are applied to the perturbed system. The FFDs (full field displays) of coupling paired Zernike terms (Z5&Z6, Z7 @ Z8 and Z10 @ Z11) before correction are shown in Fig. 7(a)-(c). The FFDs of coupling paired Zernike terms after correction are illustrated in Fig. 7(d)-(f). It can be seen that these representative aberration fields can be almost recovered to the nominal design states based on the approach proposed above.

The point spread function (PSF) of the off-axis two-mirror system in the nominal design states is shown in Fig. 8(a) and Fig. 8(d). The PSF of the perturbed off-axis system before correction is presented in Fig. 8(b) and Fig. 8(e). The PSF of the perturbed system after correction is illustrated in Fig. 8(c) and Fig. 8(f). It can be seen that the PSF can also be almost recovered to the nominal states based on the approach presented above.

To further verify the validity of the proposed method, Monte-Carlo simulations will be carried out for the off-axis two-mirror system. Four representative cases are used in the simulations and they are listed in Table 4. The ranges of component perturbations increase by degrees without the corresponding measurement errors in Case 1, 2 and 3. The disturbance ranges in case 4 are identical to that in case 3, but the corresponding relative measurement errors are 2 %.

The 400 experimental perturbations are generated randomly for all cases and followed uniform distribution. Based on the proposed approach, the simulation for each perturbation state can be carried out. The perturbation values can be determined for each trial system. Then the correction values are adopted to correct the off-axis telescope. In each case, the root-mean-square errors (RMSEs) are utilized to evaluate the validity and accuracy of the presented approach, which can be given by

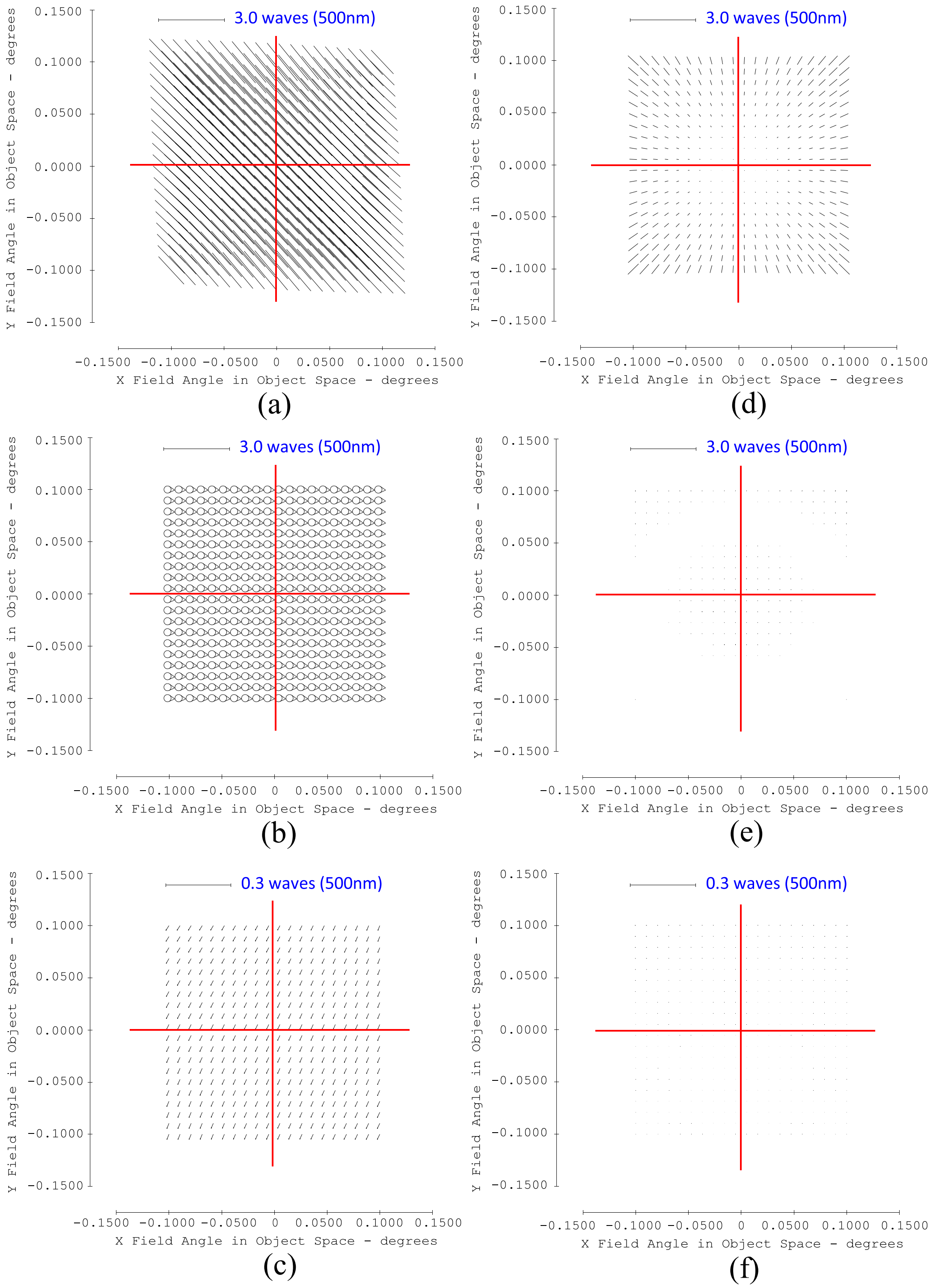

Fig. 7. (a) Full field displays (FFDs) of Z5 @ Z6 term before system correction; it contains the influences of misalignments and mirror figure errors. (b) FFDs of Z7 @ Z8 term before system correction. (c) FFDs of Z10 @ Z11 term before system correction. (d) FFDs of Z5 @ Z6 term after system correction. (e) FFDs of Z7 @ Z8 term after system correction. (f) FFDs of Z10 @ Z11 term after system correction.

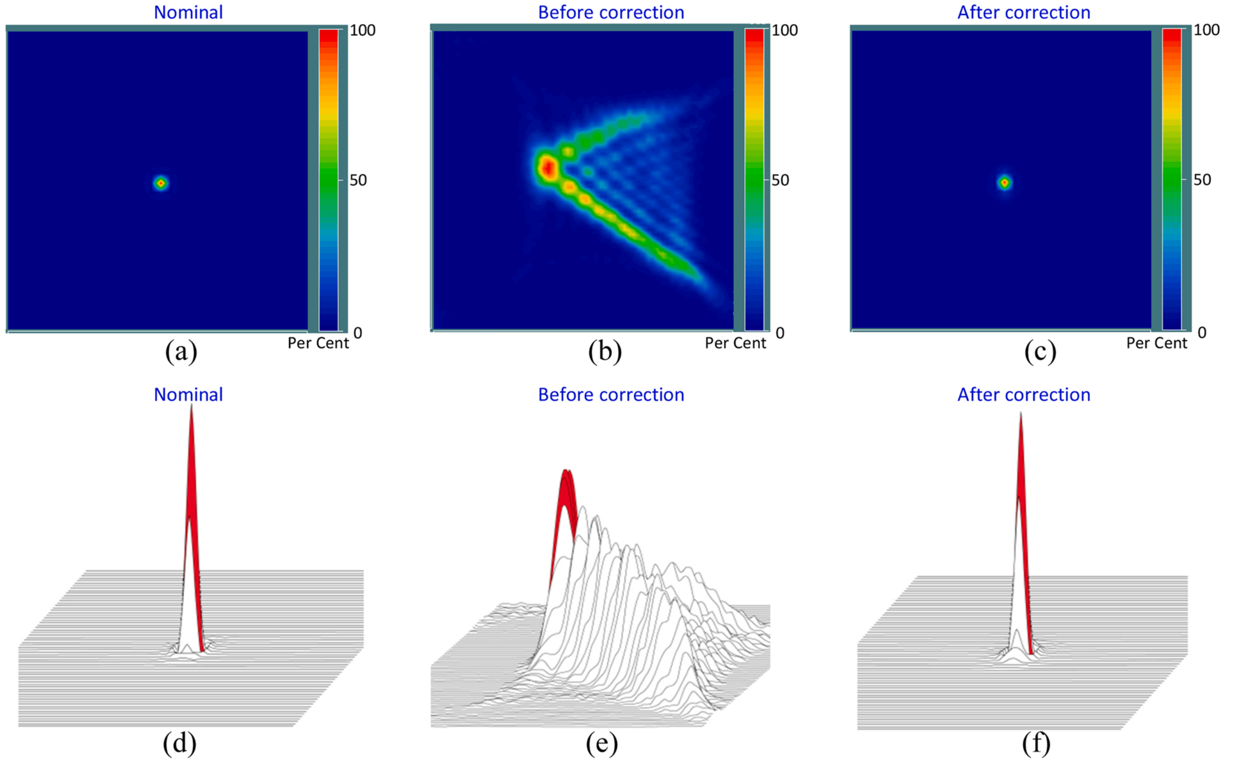

Fig. 8. Point spread function (PSF) for central field. The "Nominal" represents PSF of the original system. The "Before correction" stands for PSF of the perturbed system. The "After correction" stands for PSF of the corrected system. (a) and (d) for PSF in the nominal state. (b) and (e) for PSF before correction. (c) and (f) for PSF after correction.

Table 4
Four Representative Cases used in the Simulations.

	XDE_{SM}, YDE_{SM}	ADE_{SM}, BDE_{SM}	${}_{F}C_i^{PM/SM}$	Measurement errors
Case 1	[− 0.2,0.2]	[− 0.01,0.01]	[− 0.06,0.06]	\
Case 2	[− 0.5,0.5]	[− 0.02,0.02]	[− 0.1,0.1]	\
Case 3	[− 1.0,1.0]	[− 0.05,0.05]	[− 0.3,0.3]	\
Case 4	[− 1.0,1.0]	[− 0.05,0.05]	[− 0.3,0.3]	2 %

$$RMSE_j = \sqrt{\frac{1}{100}\sum_{n=1}^{100}\left[X_j(n) - x_j(n)\right]^2}, \tag{30}$$

where $X_j(n)$ and $x_j(n)$ designate the introduced and calculated values for corresponding perturbation, j denotes the serial number of the perturbation.

The RMSEs of correction values for each case based on the method presented above are shown in Fig. 9. The abscissa of the subplots in Fig. 9 is the case number, and the ordinate is the RMSEs. The RMSEs of decenters for the SM are shown in Fig. 9(a)-(b). The RMSEs of tip-tilts for the SM are illustrated in Fig. 9(c)-(d). The RMSEs of trefoil figure errors for the SM are presented in Fig. 9(e)-(f). The RMSEs of trefoil and astigmatic figure errors for the PM are illustrated in Fig. 9(g)-(j). The Zernike coefficients are in $\lambda(\lambda = 500nm)$, the ADE_{SM} and BDE_{SM} are in degrees, the XDE_{SM} and YDE_{SM} are in mm.

As shown in Fig. 9, the accuracy of Case 1 is the highest. With increase of the perturbation ranges, the accuracy of Case 2 and 3 is also high. The corresponding results of case 1, 2 and 3 show the correctness and accuracy of the presented method. It indicates that the presented method also has good adaptability for the off-axis telescope with larger perturbations. The results of Case 4 demonstrate the approach can also be affected by the errors of measurements. But even so, the accuracy of the approach is high enough. These results demonstrate that the presented approach is an excellent choice for correction of perturbed off-axis telescopes.

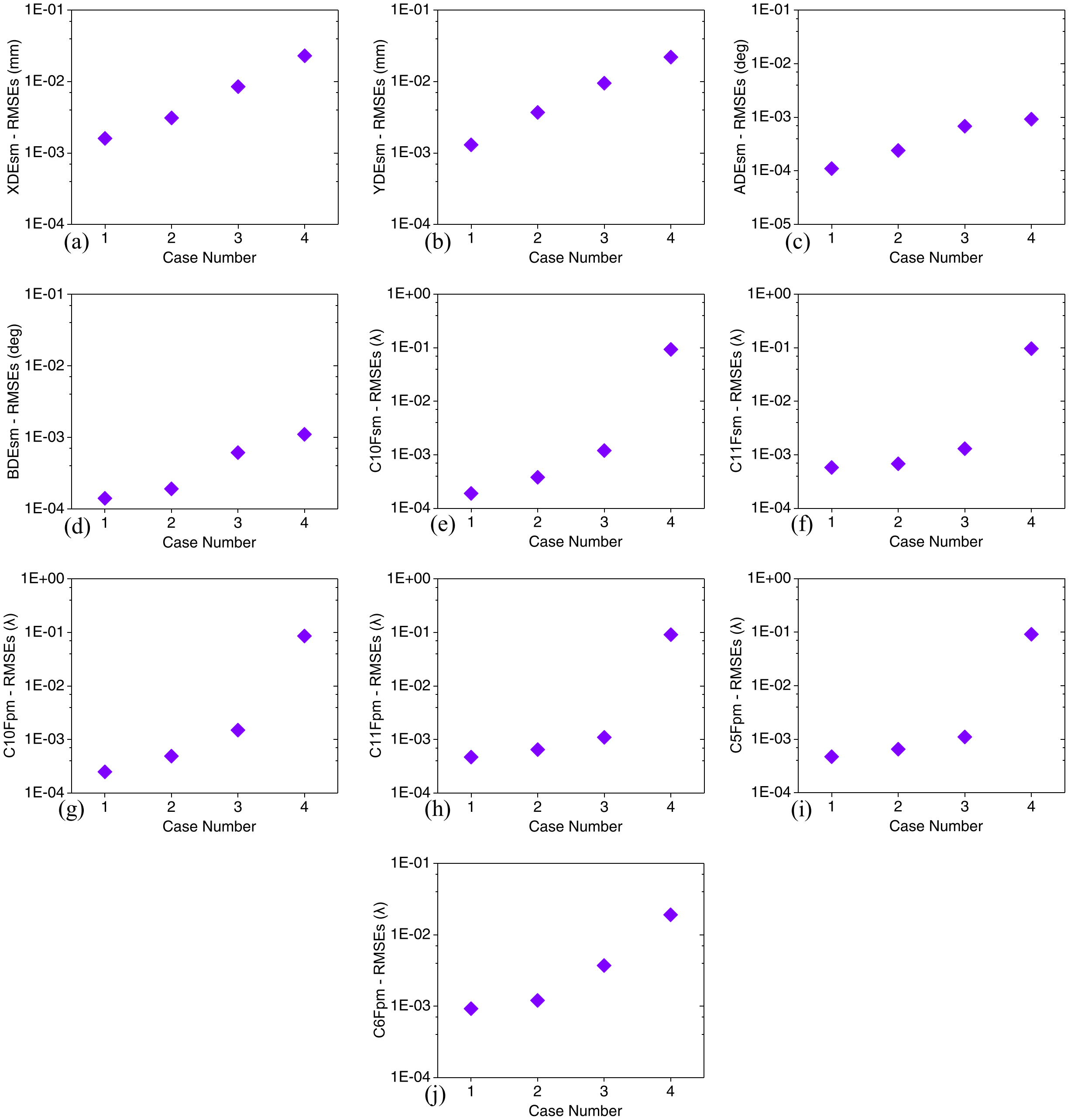

Fig. 9. RMSEs of correction values for four cases. (a), (b), (c) and (d) for the SM misalignments, (e)-(f) for surface figure errors of SM, (g)-(j) for surface figure errors of PM.

5. Conclusion

This paper was concerned with the correction strategy for pupil-offset off-axis optical telescopes with complex figure errors and misalignments on the basis of nodal aberration theory. The analytical description of the aberration contribution from complex surfaces in off-axis telescopes was obtained. It gave the unified description for the influence of complex surfaces located at the system stop and away from the stop. The correction model of off-axis telescopes with surface figure errors and misalignments was established by using the analytical description. Based on the correction model, the introduced perturbations and calculated results were almost the same. The perturbed off-axis telescopes can be almost restored to system nominal states after correction and can meet the requirements well. The results of Monte-Carlo simulations demonstrated the accuracy and effectiveness of the presented approach. The proposed correction strategy can well adapt to the off-axis telescopes with figure errors and misalignments. The correction model proposed in the paper can be further extended to include higher-order aberrations, which can adapt to the correction of higher-order aberrations induced by harsh environments. The work gave a useful reference for system correction of the pupil-offset off-axis telescopes.

Declaration of Competing Interest

The authors declare that they have no known competing financial interests or personal relationships that could have appeared to influence the work reported in this paper.

Data Availability

Data will be made available on request. Data may be obtained from the authors in this paper upon reasonable request.

Acknowledgments

This work was supported by National Natural Science Foundation of China (NSFC) (61905241, 61705223), National Key Research and Development Program of China (2016YFB0500100), ShuGuang Talents Scheme Award of Changchun Institute of Optics, Fine Mechanics and Physics, Chinese Academy of Sciences.

References

[1] R.N. Wilson, Active optics and the new technology telescope (NTT): the key to improved optical quality at lower cost in large astronomical telescopes, Contemp. Phys. 32 (3) (1991) 157–171.
[2] N. Devaney, C. Reinlein, N. Lange, M. Goy, A. Goncharov, P. Hallibert, HYPATIA and STOIC: an active optics system for a large space telescope, Proc. SPIE 9904 (2016), 990469.
[3] F. Kenny, N. Devaney, A. Goncharov, M. Goy, C. Reinlein, An active optics system for large UVOIR space telescopes, Proc. SPIE 10698 (2018), 106986C.
[4] N. Devaney, F. Kenny, A. Goncharov, M. Goy, C. Reinlein, Development of a prototype active optics system for future space telescopes, Appl. Opt. 57 (22) (2018) E101–E106.
[5] L.G. Cook, Three-mirror anastigmat used off-axis in aperture and field, Proc. SPIE 183 (1979) 207–211.
[6] H.J. Juranek, R. Sand, J. Schweizer, B. Harnisch, B. Kunkel, E. Schmidt, A. Litzelmann, F. Schillke, G. Dempewolf, Off-axis telescopes: the future generation of Earth observation telescopes, Proc. SPIE 3439 (1998) 104–115.
[7] D. Alaluf, R. Bastaits, K. Wang, M. Horodinca, G. Martic, B. Mokrani, A. Preumont, Unimorph mirror for adaptive optics in space telescopes, Appl. Opt. 57 (14) (2018) 3629–3638.
[8] S. Leitz, M. Gerhards, S. Verpoort, U. Wittrock, M. Freudling, A. Grzesik, M. Erhard, P. Hallibert, Vibration and shock testing of a 50 mm aperture unimorph deformable mirror, Proc. SPIE 11852 (2021) 1926–1933.
[9] S. Kim, H.S. Yang, Y.W. Lee, S.W. Kim, Merit function regression method for efficient alignment control of two-mirror optical systems, Opt. Express 15 (8) (2007) 5059–5068.
[10] R. Upton, T. Rimmele, R. Hubbard, Active optical alignment of the advanced technology solar telescope, Proc. SPIE 6271 (2006), 62710R.
[11] R.V. Shack, K.P. Thompson, Influence of alignment errors of a telescope system, Proc. SPIE 251 (1980) 146–153.
[12] K. Thompson, Description of the third-order optical aberrations of near-circular pupil optical systems without symmetry, J. Opt. Soc. Am. A 22 (7) (2005) 1389–1401.
[13] K.P. Thompson, Multinodal fifth-order optical aberrations of optical systems without rotational symmetry: spherical aberration, J. Opt. Soc. Am. A 26 (5) (2009) 1090–1100.
[14] K.P. Thompson, Multinodal fifth-order optical aberrations of optical systems without rotational symmetry: the comatic aberrations, J. Opt. Soc. Am. A 27 (6) (2010) 1490–1504.
[15] K.P. Thompson, Multinodal fifth-order optical aberrations of optical systems without rotational symmetry: the astigmatic aberrations, J. Opt. Soc. Am. A 28 (5) (2011) 821–836.
[16] K.P. Thompson, T. Schmid, O. Cakmakci, J.P. Rolland, Real-ray-based method for locating individual surface aberration field centers in imaging optical systems without rotational symmetry, J. Opt. Soc. Am. A 26 (6) (2009) 1503–1517.
[17] T. Schmid, J.P. Rolland, A. Rakich, K.P. Thompson, Separation of the effects of astigmatic figure error from misalignments using Nodal Aberration Theory (NAT), Opt. Express 18 (16) (2010) 17433–17447.
[18] K. Fuerschbach, J.P. Rolland, K.P. Thompson, Extending nodal aberration theory to include mount-induced aberrations with application to freeform surfaces, Opt. Express 20 (18) (2012) 20139–20155.
[19] K. Fuerschbach, J.P. Rolland, K.P. Thompson, Theory of aberration fields for general optical systems with freeform surfaces, Opt. Express 22 (22) (2014) 26585–26606.
[20] Z.H. Pang, X.W. Fan, Q.F. Chen, Z. Ma, G.Y. Zou, Influence of surface-profile error of larger mirror on aberrations characteristics of optical system, Acta Opt. Sin. 33 (4) (2013), 0422002.
[21] G. Ju, C. Yan, Z. Gu, H. Ma, Computation of astigmatic and trefoil figure errors and misalignments for two-mirror telescopes using nodal-aberration theory, Appl. Opt. 55 (13) (2016) 3373–3386.
[22] X. Zhang, S. Xu, H. Ma, N. Liu, Optical compensation for the perturbed three mirror anastigmatic telescope based on nodal aberration theory, Opt. Express 25 (11) (2017) 12867–12883.
[23] X. Zhang, D. Zhang, S. Xu, H. Ma, Active optical alignment of off-axis telescopes based on nodal aberration theory, Opt. Express 24 (23) (2016) 26392–26413.
[24] Z. Gu, C. Yan, Y. Wang, Alignment of a three-mirror anastigmatic telescope using nodal aberration theory, Opt. Express 23 (19) (2015) 25182–25201.
[25] J. Wang, B. Guo, Q. Sun, Z. Lu, Third-order aberration fields of pupil decentered optical systems, Opt. Express 20 (11) (2012) 11652–11658.
[26] H. Hu, J. Liu, Z. Fan, Interaction of pupil offset and fifth-order nodal aberration field properties in rotationally symmetric telescopes, Opt. Express 21 (15) (2013) 17986–17998.
[27] R.A. Buchroeder, 1976. Tilted component optical systems, Ph.D. dissertation (University of Arizona, Tucson, Arizona, 1976).
[28] J.C. Wyant, K. Creath, Basic wavefront aberration theory for optical metrology, in: R.R. Shannon, J.C. Wyant (Eds.), Applied Optics and Optical Engineering, Academic, 1992, pp. 1–53.
[29] M. Wen, C. Han, H. Ma, Active compensation for optimal RMS wavefront error in perturbed off-axis optical telescopes using nodal aberration theory, Appl. Opt. 60 (6) (2021) 1790–1800.
[30] M. Wen, H. Ma, C. Han, Active alignment of complex perturbed pupil-offset off-axis telescopes using the extension of nodal aberration theory, Appl. Opt. 60 (13) (2021) 3874–3887.
[31] R.W. Gray, J.P. Rolland, Wavefront aberration function in terms of R. V. Shack's vector product and Zernike polynomial vectors, J. Opt. Soc. Am. A 32 (10) (2015) 1836–1847.